Two-Dimensional Crystals and Quasicrystals in Nonlinear Optics

E. Pampaloni, P. L. Ramazza, S. Residori, and F. T. Arecchi*
Istituto Nazionale di Ottica, 50125 Firenze, Italy
(Received 28 March 1994)

We report the observation of two-dimensional periodic and quasiperiodic structures in the transverse profile of an optical beam circulating in a loop which contains a nonlinear medium. The symmetries of the patterns are imposed by an image rotation within the loop. We propose a simple model which shows the existence of two unstable bands of transverse wave vectors. Close to threshold, the predictions of the model are qualitatively and quantitatively confirmed by the experiment.

PACS numbers: 42.50.Lc, 05.45.+b

Until now, the study of pattern formation in dissipative systems has been concerned mainly with the two opposite limits of spatially periodic or spatially disordered structures [1]. Only recently a theory of two-dimensional quasiperiodic patterns in nonequilibrium systems has been offered [2], and fluid dynamics experiments of parametrically excited surface waves [3] have confirmed the existence of dynamic structures with quasicrystalline properties [4]. Another example of two-dimensional quasicrystals is given by the quasisymmetrical tiling of the phase space for a particle moving in a magnetic field [5].

In this Letter we report the first experimental evidence of the formation of two-dimensional crystal-like and quasicrystal-like structures in the transverse profile of an optical beam. These patterns are generated by the superposition of $N = 2, 3, 4, \ldots$ pairs of oppositely directed wave vectors; they display an N-fold symmetry and are characterized by a long range orientational order and self-similarity properties. However, except for the cases $N = 2, 3, 4, 6$, they have quasiperiodic rather than periodic translational order, and thus they can be classified as quasicrystals instead of crystals.

The experiment is based on the joint role of a Kerr nonlinearity and a light feedback [6]. It consists of injecting an Ar^+ laser beam in the front of a liquid crystal light valve (LCLV) and feeding the reflected light on the back after propagation. The LCLV is made of a mirror sandwiched between a nematic liquid-crystal (LC) layer in the front and a photoconductive layer in the back [7]. An ac voltage is applied across the two layers. The photoconductor changes its resistance with the intensity of the light incident on it, and the LC molecules reorient accordingly, modifying their refractive index. Thus, a phase modulation, proportional to the intensity distribution on the back, is induced on the beam reflected from the front. The reflected light travels in a loop delimited by a beam splitter, a mirror, and a fiber bundle, and including a free propagation length L where diffraction takes place. The role of diffraction is to convert phase into amplitude modulation which is then converted again into phase modulation by the LCLV. This feedback mechanism can destabilize the homogeneous state, giving rise to transverse patterns in the light intensity distribution. At the linear stage a circle of critical transverse wave vectors $|\mathbf{q}|$ becomes simultaneously unstable. Close to threshold, the pattern is determined by nonlinear interactions among wave vectors on this circle, which has a radius $q_{\mathrm{I}} = \sqrt{\pi k_0/L}$ for a focusing medium and $q_{\mathrm{II}} = \sqrt{3\pi k_0/L}$ for a defocusing medium [8], $k_0 = 2\pi/\lambda$ being the optical wave number.

The free end of the fiber bundle is mounted on a rotation stage which allows for a continuous angular positioning over a full 360° range with a high resolution (readout to 0.2°). This way, the feedback image arriving at the photoconductive layer of the LCLV can be rotated to any angle Δ. It was shown theoretically [6] and experimentally [9–11] that for $\Delta = 0$ only hexagons are stable [8]. On the other hand, for $\Delta = \pi$ it was shown that only rolls are stable and that a competition between hexagons and rolls can be achieved by inserting an attenuation filter in front of one-half of the LCLV [11].

Initially, we fix the input intensity $I_0 = 4.5$ mW/cm^2, the rms amplitude (40 V) and frequency (9 kHz) of the voltage applied and the free propagation length $L = 75$ cm, and change the rotation angle Δ in the feedback loop. When the rotation angle is exactly commensurate to 2π, that is, when $\Delta = 2\pi/N$ with $N = 2, 3, 4, \ldots$, a pattern with an N-fold symmetry develops. The symmetry is induced by the rotation angle in the feedback, and it is not due to boundary effects that arise when the system is strongly limited in its transverse extension [12,13].

In Fig. 1(a) we report different near-field patterns, obtained by imaging on a change coupled device (CCD) camera the front of the LCLV, for various rotation angles $\Delta = 2\pi/N$, where N is changed from 2 to 9. Since the critical wavelength is of the order of 1 mm and the LCLV has a diameter of 3 cm, a central region with negligible boundary influences has been observed up to N of the order of 20. Looking at the edge, it can be seen that away from the center the system tends to stabilize rolls for N even and hexagons for N odd. In fact, the feedback rotation constraint is more efficient close to the center, whereas at the edge the patterns recover the two basic symmetries corresponding to $\Delta = 0$ (N odd) and $\Delta = \pi$ (N even) [11].

 0031-9007/95/74(2)/258(4)$06.00

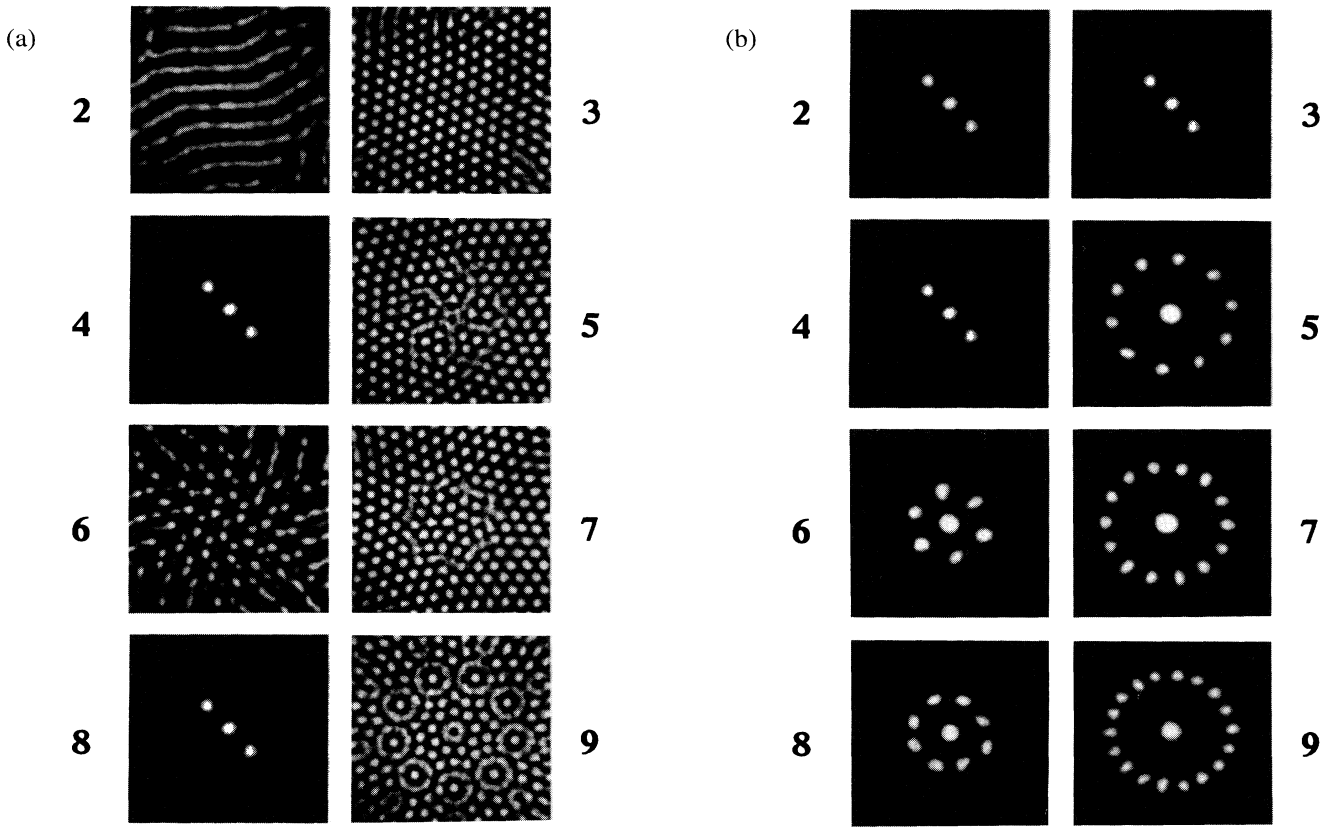

FIG. 1. Experimental patterns observed for feedback rotation angles $\Delta = 2\pi/N$. The N values are indicated close to each frame. (a) Near-field patterns. (b) Far-field patterns; all frames correspond to the same magnification, thus the rings with N even and those with N odd are, respectively, proportional to q_{I} and q_{II}.

The far-field patterns [Fig. 1(b)], collected on the focus of a lens, are the power spectra of the corresponding near-field images and provide directly the number of modes involved in the pattern formation and the length of the critical wave vector (radius of the ring where the peaks are located). The patterns on the first and second column (respectively, N even and odd) have different lengths of the critical wave vector. Taking into account the optical magnification of the system, we measure $q_{\mathrm{II}} = 12.5\ \mathrm{mm}^{-1}$ for N odd and $q_{\mathrm{I}} = 7.3\ \mathrm{mm}^{-1}$ for N even, so that the ratio $q_{\mathrm{II}}/q_{\mathrm{I}}$ is close to $\sqrt{3}$, in agreement with the critical wave numbers ratio of a defocusing to a focusing medium [8]. Indeed, even though the LCLV acts as a defocusing medium, also an instability with the q_{I} of a focusing medium can be excited, as shown in Ref. [11]. The fact that for any pattern each $\mathbf{q}$ component contributes as a pair of opposite directions gives rise to $2N$ peaks for N odd, but only to N peaks for N even.

A linear stability analysis explains the presence of two different critical wave vectors when a rotation is introduced in the feedback path. Starting from the model of a Kerr slice feedback [6,8], we modify the equation for the refractive-index modulation n induced in the material in the following way:

$$\frac{\partial n}{\partial t} + n + l_D^2 \nabla_\perp^2 n = -\chi R[I(r,\theta)], \tag{1}$$

where the time has been normalized to the response time of the LCLV, l_D is the material diffusion length, and $\chi > 0$ (defocusing medium) is the strength of the nonlinearity. $I(r,\theta)$ is the feedback intensity, (r,θ) are the transverse polar coordinates, and R is the rotation operator $R[I(r,\theta)] = I(r,\theta + \Delta)$.

Since the response time of the LCLV is a few ms while the round-trip time is a few ns, the field can be considered at any instant in equilibrium with the material perturbations. Thus Eq. (1) has to be coupled with the stationary field propagation within the material, where the field acquires a phase factor e^{-in} and over the length L, which is accounted for by the phase operator [8] $e^{-i(L/2k_0)\nabla^2}$. Therefore the right-hand side of Eq. (1) is written in operator form as

$$R[I(r,\theta)] = I_0 |e^{-i\frac{L}{2k_0}\nabla^2} e^{-in(r,\theta+\Delta)}|^2. \tag{2}$$

Notice that for $L = 0$ (no free propagation) this reduces to

I_0. In this case, a phase to amplitude conversion requires an interference between input and feedback light, so that the square in Eq. (2) is replaced by [7] $|1 + \alpha e^{-in(r,\theta+\Delta)}|^2$, α being an attenuation constant in the feedback loop. This latter situation was studied by a linear stability analysis in Ref. [14]. We apply a similar approach to our case.

Precisely, we suppose that the homogeneous solution is perturbed by a phase modulation of wave vector $\mathbf{q}$ and that the feedback rotation of an angle $\Delta = 2\pi/N$ excites N vectors with the same length in N directions spaced by the angle Δ. Therefore, the phase perturbation can be expanded as $n = \sum_{j=1}^{N} a_j \cos\mathbf{q}_j \cdot \mathbf{r}$. The $\mathbf{q}$ vectors are related by the rotation operator in such a way that $R\mathbf{q}_j = \mathbf{q}_{j+1}$. With this expansion, the propagation over a distance L of a field gives rise to the following feedback intensity:

$$I(L,\mathbf{r},t) = I_0[1 + 2\,\sin\left(\frac{q^2L}{2k_0}\right)\sum_{j=1}^{N} a_j\,\cos\mathbf{q}_j \cdot \mathbf{r}]. \quad (3)$$

Substituting this expression into Eq. (1), we evaluate the eigenvalues λ_j of the perturbation vector $(a_1, a_2, \ldots, a_N)$ as $\lambda_j = -(1 + l_D^2 q^2) + \chi I_0 \sin q^2 L/2k_0 [e^{iN\pi}]_j^{1/N}$, where $[\cdots]_j^{1/N}$ denotes the jth Nth root of the unity. By selecting the eigenvalues with maximal real part, we derive two marginal stability curves

$$\text{branches I:}\quad \chi I_{\text{th}} = \begin{cases} \dfrac{1 + l_D^2 q^2}{\sin(q^2L/2k_0)} & \text{for } N \text{ even}, \\ \dfrac{1 + l_D^2 q^2}{\cos(\Delta/2)\,\sin(q^2L/2k_0)} & \text{for } N \text{ odd}, \end{cases} \quad (4)$$

$$\text{branches II:}\quad \chi I_{\text{th}} - \frac{(1 + l_D^2 q^2)}{\sin(q^2L/2k_0)} \quad \text{for } N \text{ even or odd}. \quad (5)$$

The positive branches of these two curves give the value I_{th} of the input intensity I_0 necessary to excite an instability with a spatial frequency q. In the diffractive limit, $l_D^2 \ll \lambda L$, all branches have their minima at $q^2L/2k_0 = (2n + 1)\pi/2$, with $n = 0, 2, \ldots$ (even integer) for branches I and $n = 1, 3, \ldots$ (odd integer) for branches II, so that, with respect to the first critical wave number $q_{\text{I}} = \sqrt{\pi k_0/L}$, the next is located at $q_{\text{II}} = \sqrt{3}\,q_{\text{I}}$ and the higher ones at $\sqrt{5}\,q_{\text{I}}$, $\sqrt{7}\,q_{\text{I}}, \ldots$. Close to threshold, only the first two branches of I and II [reported in Fig. 2(a)] are involved in the wave number selection process since they have the lowest minima. Furthermore, for N odd, branch I depends on N through Δ; hence its minimum can be above or below that of branch II. At threshold, the lowest local minimum determines the excited mode.

Comparing the magnitude of the real parts of the two unstable eigenvalues, it results that for N even, the excited mode is always the one with q_{I}, independently of N. On the other hand, for N odd, branch I has an enhancement

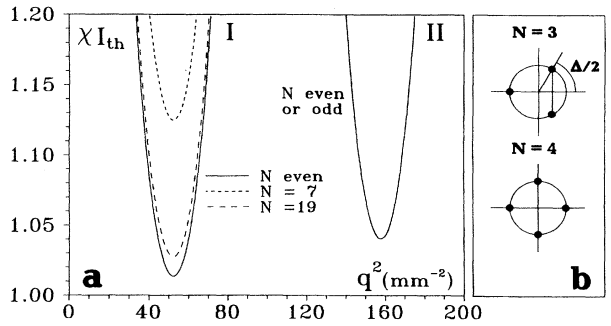

FIG. 2. (a) Marginal stability curves evaluated for $L = 75$ cm and $l_D = 15.5$ μm. The first branch has the lowest threshold for any N if N is even and also for N odd if N is large. For N odd and small the second branch has a lower threshold. (b) The N roots of the unity in the complex plane, for $N = 3$ and 4. For $N = 3$ it is easy to realize the enhancement factor $1/\cos(\Delta/2)$ reported in Eq. (4) for N odd.

factor $1/\cos(\Delta/2)$ [see Eq. (4)], which is larger for lower N, as shown for $N = 3$ in Fig. 2(b), and hence branch II is favored, whereas for high values of N it exists a pair of eigenvalues closest to the real axis, for which branch I can still have the lower threshold. For intermediate N the minima of branch I and II can be aligned, and this occurs, in the diffractive limit, for

$$\frac{\pi}{N_T} = \arccos\left(\frac{1 + l_D^2 q_{\text{I}}^2}{1 + l_D^2 q_{\text{II}}^2}\right). \quad (6)$$

In order to verify the validity of this relation, we proceed in the following way: For a given propagation length L we adjust the pump intensity I_0 in such a way that the system is just above threshold, then, starting at $N = 3$, we analyze the pattern for different feedback rotation angles $\Delta = 2\pi/N$, incrementing N by steps of 2. Looking at the far field, we take as a transition point between the two unstable bands that for which a second ring develops inside

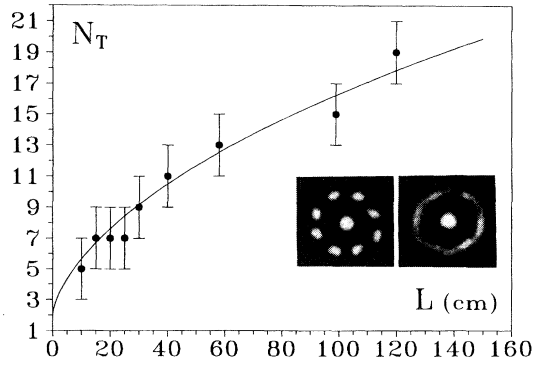

FIG. 3. Measured values N_T as a function of the free propagation length L. The best fit line corresponds to $l_D = 15.5$ μm. In the inset the far-field patterns, for $L = 30$ cm and $N = 8$ (left) and 9 (right), show that, at variance with the previous figure, here the ring has the same radius q_{I} in both cases, as expected from the N_T curve.

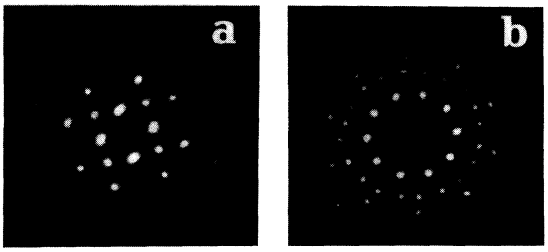

FIG. 4. Far-field patterns in the nonlinear regime (input intensity 5 times above threshold). To avoid saturation, the central region has been filtered out. In case (a), ($N = 4$) there is evidence of nonlinear peaks arranged on a periodic lattice. In case (b), ($N = 5$) secondary and tertiary peaks correspond to wave numbers close, respectively, to $\sqrt{7/3}$ and $\sqrt{11/3}$ times that (q_{II}) of the main peaks.

the first one. Since the transition is not sharp and there are intermediate situations in which both wavelengths coexist, the N_T measured this way has an error bar ± 2. Repeating the operation for various lengths L, we plot N_T vs L. The experimental data (Fig. 3) are fitted with a line resulting from Eq. (6) with l_D as a free parameter. The best fit provides $l_D = 15.5\ \mu$m. The inset of Fig. 3 shows the experimental far-field patterns at $L = 30$ cm and $N = 8$ and 9. In the odd case, since the pair of complex roots closest to the real axis provides a lower threshold at q_I, we have the same radius as for the even case; however, the imaginary parts of the eigenvalues add a rotation in time, and hence the peaks are not resolved.

The quasiperiodicity in the far field patterns is already provided by the leading components with equal moduli [Fig. 1(b)] whenever the projections of two successive wave vectors are irrational on any symmetry axis, that is, for $N = 5, 7, 8, 9, \ldots$ [3]. The nonlinearity of the medium should also provide combination peaks. Indeed, far above threshold, we observe further peaks which lie either on a regularly spaced or on a self-similar lattice (Fig. 4), depending on whether they refer to a periodic or quasiperiodic structure. For $N = 5$, the secondary and tertiary peaks are located close to $\sqrt{7/3}$ and $\sqrt{11/3}$ times the primary peaks. These values indeed correspond to minima of higher stability bands, and thus they are slightly different from the ideal values 1.618... and 2 [4]. Further details on the nonlinear regime will be reported elsewhere.

We acknowledge F. Papoff for fruitful discussions. This work has been partially supported by the EEC-Esprit Basic Research action TONICS (Contract No. 7118).

*Also at the Physics Department, University of Florence, Italy.

[1] See, for example, M. C. Cross and P. C. Hohenberg, Rev. Mod. Phys. **65**, 851 (1993).
[2] B. A. Malomed, A. A. Nepomnyaschiĭ, and M. I. Tribelskiĭ, Sov. Phys. JETP **69**, 388 (1989).
[3] B. Christiansen, P. Alstrøm, and M. T. Levinsen, Phys. Rev. Lett. **68**, 2157 (1992); W. S. Edwards and S. Fauve, Phys. Rev. E **47**, 788 (1993).
[4] D. Shechtman, I. Blech, D. Gratias, and J. W. Cahn, Phys. Rev. Lett. **53**, 1951 (1984); D. Levine and P. J. Steinhardt, Phys. Rev. Lett. **53**, 2477 (1984).
[5] V. V. Beloshapkin, A. A. Chernikov, R. Z. Sagdeev, and G. M. Zaslavsky, Phys. Lett. **A 133**, 395 (1988); A. A. Chernikov, R. Z. Sagdeev, D. A. Usikov, and G. M. Zaslavsky, Comput. Math. Applic. **17**, 17 (1989).
[6] W. J. Firth, J. Mod. Opt. **37**, 151 (1990); G. D'Alessandro and W. J. Firth, Phys. Rev. Lett. **66**, 2597 (1991).
[7] S. A. Akhmanov, M. A. Vorontsov, V. Yu. Ivanov, A. V. Larichev, and N. I. Zheleznykh, J. Opt. Soc. Am. B **9**, 78 (1992).
[8] G. D'Alessandro and W. J. Firth, Phys. Rev. A **46**, 537 (1992).
[9] R. Macdonald and H. J. Eichler, Opt. Commun. **89**, 289 (1992).
[10] M. Tamburrini, M. Bonavita, S. Wabnitz, and E. Santamato, Opt. Lett. **18**, 855 (1993).
[11] E. Pampaloni, S. Residori, and F. T. Arecchi, Europhys. Lett. **24**, 647 (1993).
[12] F. Papoff, G. D'Alessandro, G. L. Oppo, and W. J. Firth, Phys. Rev. A **48**, 634 (1993).
[13] E. Pampaloni, P. L. Ramazza, S. Residori, and F. T. Arecchi, Europhys. Lett. **25**, 587 (1994).
[14] H. Adachihara and H. Faid, J. Opt. Soc. Am. B **10**, 1242 (1993).

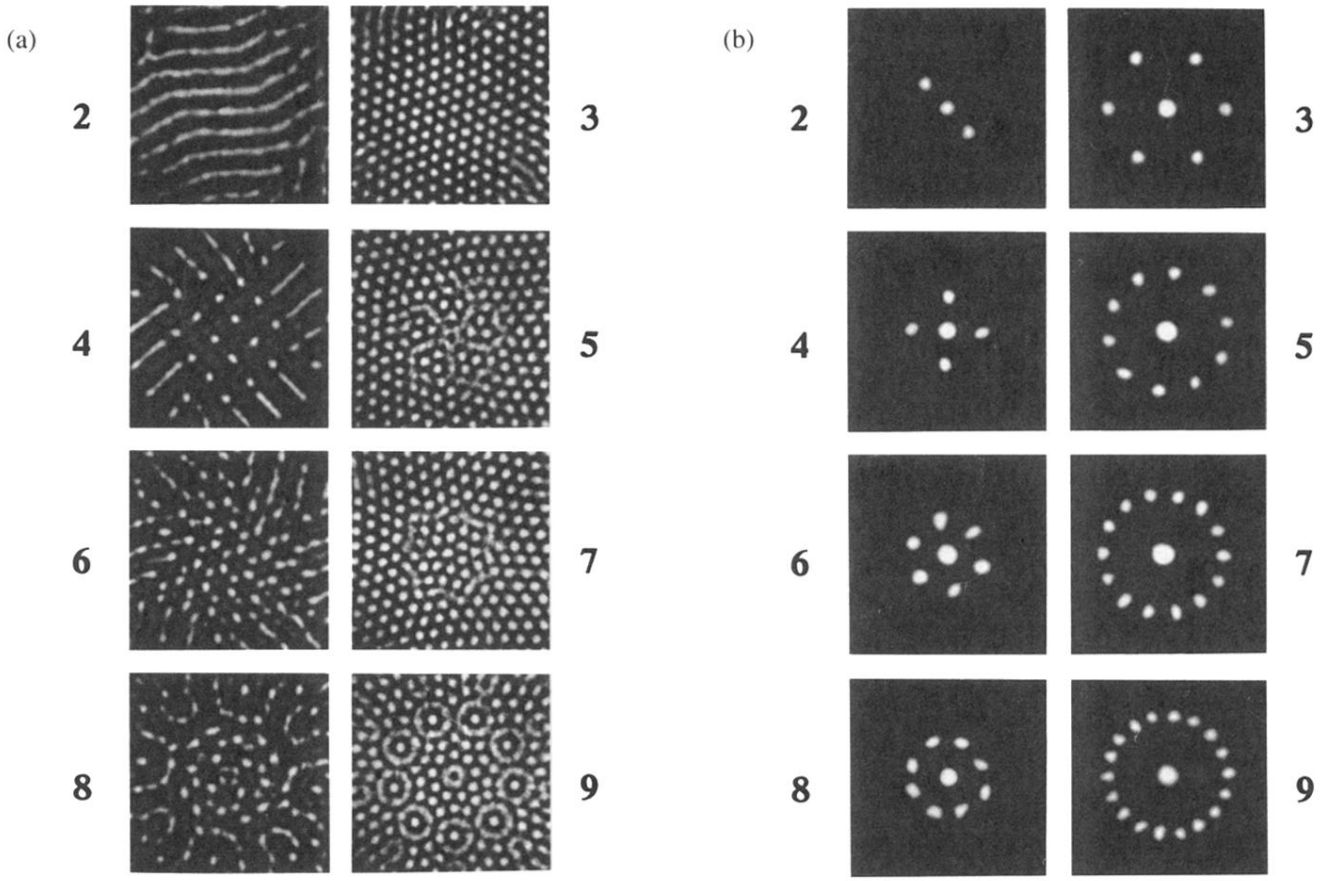

FIG. 1. Experimental patterns observed for feedback rotation angles $\Delta = 2\pi/N$. The N values are indicated close to each frame. (a) Near-field patterns. (b) Far-field patterns; all frames correspond to the same magnification, thus the rings with N even and those with N odd are, respectively, proportional to q_{I} and q_{II}.

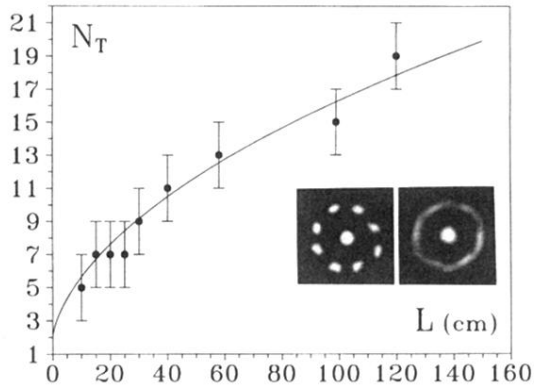

FIG. 3. Measured values N_T as a function of the free propagation length L. The best fit line corresponds to $l_D = 15.5\ \mu$m. In the inset the far-field patterns, for $L = 30$ cm and $N = 8$ (left) and 9 (right), show that, at variance with the previous figure, here the ring has the same radius q_1 in both cases, as expected from the N_T curve.

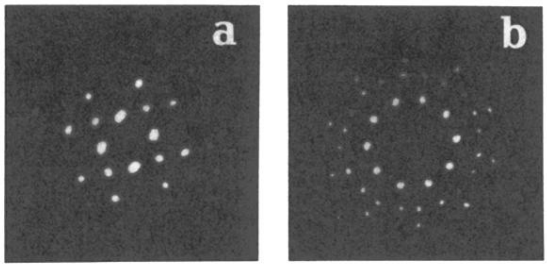

FIG. 4. Far-field patterns in the nonlinear regime (input intensity 5 times above threshold). To avoid saturation, the central region has been filtered out. In case (a), ($N = 4$) there is evidence of nonlinear peaks arranged on a periodic lattice. In case (b), ($N = 5$) secondary and tertiary peaks correspond to wave numbers close, respectively, to $\sqrt{7/3}$ and $\sqrt{11/3}$ times that (q_{11}) of the main peaks.